# Spatial focusing and intersymbol interference in multiple-input/single-output time reversal communication systems

Peter Blomgren, Persefoni Kyritsi, Arnold D. Kim, and George Papanicolaou

***Abstract*— We study a multiple-input/single-output underwater communication system that applies time reversal to transmit signals so that they focus spatially and compress temporally on the intended receiver. Our simulations model an underwater acoustic channel as a waveguide, and we investigate the cases of a waveguide both with and without random inhomogeneities. We investigate physical time reversal metrics and communications related performance indicators. The results of our simulations show that spatial focusing depends strongly on the delay spread, as has been seen in experiments. This physical property of time reversal could be exploited in communication systems where signal coherence is desired only at the receiver location. However, in the simulations we find that while spatial compression increases with delay spread in a robust way (i.e. even when inhomogeneities exist), time compression does not increase with delay spread. Moreover physical measures of the temporal compression (temporal peak-to-sidelobe ratio) do not improve with waveguide inhomogeneities. Nevertheless, time reversal *reduces* intersymbol interference at the receiver as delay spread increases for both types of waveguides, which is an important effect for efficient, high speed communication. In addition to time reversal, pre-equalization at the transmitter can ideally eliminate intersymbol interference without significantly affecting spatial compression. However, this pre-equalization causes a reduction of received power, which may be acceptable when the signal to noise ratio at the receiver is high.**

***Index Terms*— Underwater acoustic communications, time reversal, waveguides, low probability of intercept, intersymbol interference.**

## I. Introduction

WITH time reversal (TR) it is possible to focus spatially and compress temporally broadband signals through a richly scattering environment [1], [2]. This involves two stages. In the first (channel estimation) stage, a source emits a short pilot signal. This signal propagates in a richly scattering medium. Its response is recorded by each element of an array that will act as a transmitter in the data transmission stage. The duration of each of these recorded signals is significantly longer than the initial pilot pulse due to multiple scattering. The second stage is the actual data transmission. In this stage, all the elements of the transmitter array send the same data stream, and each one filters the signal to be transmitted through a *time-reversal filter, i.e.* a filter that has the form of the pilot signal recorded at that particular element during the first stage but reversed in time, *i.e.* the first portion recorded becomes the last portion transmitted. These transmitted signals focus sharply in space and compress tightly in time at the source location.

Extensive laboratory TR experiments have shown this spatial focus and temporal compression across a broad range of settings (see [3] and references contained within). In each of these experiments, spatial focusing and temporal compression occur robustly, with respect to changing the complex, time-invariant, propagation medium. This robustness comes from the self-averaging properties of broadband time reversed signals that have been analyzed theoretically for acoustic wave propagation in a random medium [4].

Much research activity has been dedicated to using TR for multiple-input/single-output (MISO) underwater communication experiments. In fact, these experiments have demonstrated MISO-TR communications to be feasible [5]–[10]. Robust spatial focusing and temporal compression have been observed despite potential errors caused by several factors such as the dynamically changing ocean and system noise. Similarly, single-input/multiple-output (SIMO) systems that use passive-phase conjugation (the passive complement to MISO-TR), have been shown to work well in the ocean [11].

Since TR produces signals that are compressed in time at the receiver, it provides a mechanism for reducing intersymbol interference (ISI). In addition, because TR produces signals that focus sharply in space at the intended receiver, MISO-TR systems have potential use in situations where signal coherence is required at the receiver location and should deteriorate around it. In the present paper we show that there is indeed a rapid loss of coherence in the neighborhood around the Rx, as reflected by a dramatic increase in the bit-error-rate. This indicates a decline in detectability, at least for listening devices comparable with Rx. We present this feature as an indication of low probability of intercept (LPI). We note that the potential for LPI can only be claimed for comparable technologies, *i.e.* an eavesdropper with superior technology and/or resources cannot be prevented from intercepting the message.

In this paper we study the advantages gained by MISO-TR

Manuscript Draft: April 23, 2008

P. Blomgren is an Assistant Professor at the Department of Mathematics and Statistics of San Diego State University, San Diego, CA 92192-7720, USA (email: blomgren@mail.sdsu.edu)

P. Kyritsi is an Assistant Research Professor at the Department of Communication Technology of Ålborg University, Ålborg, Denmark. Part of this work was conducted while she was visiting the Department of Mathematics of Stanford University, Stanford, CA 94305-2125 (email: persa@kom.aau.dk)

A. D. Kim is an Associate Professor in the School of Natural Sciences at University of California, Merced, Merced, CA 95344, USA (email: adkim@umerced.edu)

G. Papanicolaou is a Professor at the Department of Mathematics of Stanford University, Stanford, CA 94305-2125, USA (email: papanico@math.stanford.edu)

communication under the following assumptions:

- The transmitting array has perfect channel state information (CSI).
- The environment is static, *i.e.* the channel is the same during both stages of the TR process.
- The receiver does not utilize an equalizer and just samples the signal while the transmitter can, in addition to time reversal, do pre-equalization.

Using numerical simulations in a waveguide, we investigate spatial focusing and temporal compression in a MISO-TR communication system. The parameter that we vary is the delay spread (DS) of the channel for a given system bandwidth B [13]. Moreover we investigate MISO-TR in channels with and without random inhomogeneities. We show that spatial focusing is indeed robust, not only with respect to substituting the random media, but also with respect to pre-equalization aimed at suppressing intersymbol interference. The quality of spatial focusing increases as the delay spread-bandwidth (DS·B) product increases.

Moreover, we show that a MISO-TR system leads to a rapid loss of coherence in the neighborhood around the Rx, as reflected by a dramatic increase in the bit-error-rate. For example, our simulation results show that at a distance of one wavelength away from the intended receiver, in the cross-range direction, one cannot reliably decode the transmitted bitstream.

We show that the quality of temporal compression at the focus point measured by physical indicators such as the temporal peak-to-sidelobe ratio depends only slightly on DS·B. By examining communications related indicators, such as ISI, more carefully, we show that TR does not eliminate ISI. Although the temporal side lobes are reduced, the equivalent channel impulse response is non-zero at the sampling times of the received signals, and therefore the symbols in the transmitted stream interfere with each other. Therefore, equalization at the receiver may still be needed for this communication system, especially in the case of channels with low DS·B, high modulation order and/ or low signal to noise ratio. We consider an extension to this MISO-TR system that pre-equalizes the channel at the transmitter in the zero-forcing sense. We show that this pre-equalization yields a channel nearly free of ISI without sacrificing spatial focusing, but at the cost of significant power reduction.

The remainder of this paper is organized as follows. In Section II we discuss the MISO-TR system. In Section III we discuss our numerical simulations to model the communication channel. In Section IV we show results from numerical simulations. We propose a pre-equalization scheme that extends this MISO-TR system to remove ISI in Section VI. The conclusions are in Section VII.

## II. MISO-TR System

### A. Fundamentals of MISO-TR systems

We describe the operation of a MISO-TR system as a two-stage process. The first stage is the channel estimation stage: the intended receiver (Rx) sends a pilot signal, and each element in the linear transmitting array (Tx) records the convolution of this pilot signal with the channel impulse response. The second stage is the actual data transmission. The Tx uses the channel state information it acquired during the channel estimation stage to transmit a bitstream that focuses spatially and is compressed temporally on the Rx.

In the remainder of the paper, we denote functions of time with lower case letters, whereas upper case indicates their frequency-domain representation.

*1) Channel estimation stage in a MISO-TR system operation:* During the first stage of the operation of a MISO-TR system, the Rx sends a pilot signal into the channel. Let $p(t) = \phi(t)e^{i2\pi f_0 t}$ denote this pilot signal. The pulse shaping function $\phi(t)$ is a low-pass signal, bandlimited to bandwidth B ($\Phi(f) = 0, |f| > B/2$), and we assume for simplicity that it is normalized to unit power. To produce the pilot symbol $p(t)$, $\phi(t)$ is modulated at a carrier frequency $f_0$, and therefore the pilot signal has spectral content in $[f_0 - B/2, f_0 + B/2]$ (for simplicity we only look at $f > 0$, *i.e.* at the analytic equivalent of the signals).

We model the channel as a linear, time-invariant filter. For that case, the signal $s_m(t)$ recorded by the $m$-th of the $M$ elements of the Tx, is given by

$$s_m(t) = h_m(t) \otimes p(t), \quad m = 1, \ldots, M, \tag{1}$$

with $\otimes$ denoting the convolution operation and $h_m(t)$ denoting the channel impulse response from the source to the $m$-th element of the Tx. By Fourier transforming (1), we obtain the frequency domain representation $S_m(f)$ of the recorded signal $s_m(t)$

$$\begin{aligned} S_m(f) &= H_m(f)P(f), \\ &= H_m(f)\Phi(f - f_0), \quad m = 1, \ldots, M. \end{aligned} \tag{2}$$

Here, $H_m(f)$ is the channel transfer function from the source to the $m$-th element of the Tx array. Due to reciprocity, it is also the channel transfer function from the $m$-th element of the Tx array to the Rx.

When the Rx sends $p(t)$ for each of the $M$ elements of the Tx to record, the Tx acquires channel state information (CSI). We assume that the noise in the channel estimation stage is negligible and the CSI is perfect.

*2) Data transmission stage in a MISO-TR system operation:* Let $x(t)$ be the signal to be transmitted. In the second stage of the MISO-TR system, each of the $M$ elements of Tx transmits simultaneously the same signal $x(t)$, by filtering it through the time reversed copy of the signal $s_m(t)$ it recorded. Here, $\overline{(\cdot)}$ denotes the complex conjugate of the argument $(\cdot)$, This operation is equivalent to by filtering $x(t)$ through $\overline{s_m(-t)}$ or equivalently, by modulating the spectrum of $X(f)$ (the Fourier transform of $x(t)$) with the phase-conjugated spectrum of the recorded $S_m(f)$.

$x(t)$ is given by

$$x(t) = \sum_{k=-\infty}^{\infty} \beta_k \delta(t - kT_s) \tag{3}$$

Here $T_s$ is the symbol period and it denotes the time by which consecutive symbols $\beta_k$ are separated. The quantity $\beta_k$ denotes the mapping of the data stream $b_k$ for the modulation scheme used. For example, for binary phase shift-keying (BPSK), bits

$b_k = 0$ or $b_k = 1$ map to $\beta_k = -1$ or $\beta_k = +1$, respectively. The spectrum $X(f)$ of $x(t)$ is given by

$$X(f) = \sum_{k=-\infty}^{\infty} \beta_k e^{i2\pi f k T_s} \tag{4}$$

The received signal at the Rx is $y(t)$ can be written as

$$y(t) = \sqrt{P} A \sum_{m=1}^{M} h_m(t) \otimes \overline{s_m(-t)} \otimes x(t). \tag{5}$$

Here, $\overline{(\cdot)}$ denotes the complex conjugate of the argument $(\cdot)$, $P$ is the transmitted power and $A$ is a normalization factor given below by (9). In the frequency domain we can write

$$\begin{aligned} Y(f) &= \sqrt{P} A \sum_{m=1}^{M} H_m(f) \overline{S_m(f)} \sum_{k=-\infty}^{\infty} \beta_k e^{i2\pi f k T_s} \\ &= \sqrt{P} H_{\text{eq}}(f) \sum_{k=-\infty}^{\infty} \beta_k e^{i2\pi f k T_s}. \end{aligned} \tag{6}$$

We define the equivalent channel transfer function $H_{\text{eq}}(f)$ as

$$H_{\text{eq}}(f) = A H_{TR}(f) \overline{\Phi(f - f_0)}. \tag{7}$$

where

$$H_{\text{TR}}(f) = \sum_{m=1}^{M} H_m(f) \overline{H_m(f)} = \sum_{m=1}^{M} |H_m(f)|^2 \tag{8}$$

The normalization factor $A$ is introduced in the previous equations in order to guarantee that the total transmitted power is $P$. $A$ is given by

$$A = \left[ \sum_{m=1}^{M} \int_B H_m(f) \overline{H_m(f)} \mathrm{d}f \right]^{-1/2}. \tag{9}$$

With this normalization factor, the time-reversal filters do not introduce any power amplification.

The inherent assumption in the formulation above is that the channel transfer functions have not changed in the data transmission stage relative to the channel estimation stage. This simplification is valid in slowly varying environments, or when the channel estimation is repeated and the channel state information is updated frequently. The effect of time-varying channels requires additional considerations.

By the properties of TR in richly scattering media, the signal $y(t)$ is expected to focus spatially at the Rx and compress temporally.

### *B. Temporal Compression*

The received signal $y(t)$ is down-converted from the carrier frequency to baseband and then sampled at integer multiples of the symbol period $T_s$. Each symbol ideally should not interfere with previous or subsequent symbols. However in reality when the Tx sends a long bitstream and the channel impulse response is not a single pulse but a series of delayed and attenuated pulses, each sampled symbol at the Rx is affected by all symbols transmitted prior to and after that one. Ideally, we would like the baseband equivalent channel impulse response $h_{eq,bb}(\mathbf{r}_{\text{Rx}}, t)$ to satisfy

$$h_{eq,bb}(\mathbf{r}_{\text{Rx}}, t = kT_s) = 0, \quad k \neq 0. \tag{10}$$

The extent to which this happens depends on both $\phi(t)$ and $h_{\text{TR}}(t)$. To measure how far we are from the ideal conditions, we define inter-symbol interference (ISI) as our metric:

$$\text{ISI} = \frac{1}{|h_{eq,bb}(\mathbf{r}_{\text{Rx}}, 0)|^2} \sum_{k \neq 0} |h_{eq,bb}(\mathbf{r}_{\text{Rx}}, kT_s)|^2. \tag{11}$$

Here, $t = 0$ corresponds to the arrival time of the sample to be decoded. ISI is the sum of powers contained in all symbol times except for $t = 0$ divided by the power at $t = 0$. It is desirable to have as low ISI as possible, because that would indicate that individual symbols can be successfully decoded by simply sampling the received signal at the appropriate instants. Equation (11) defines ISI by the sum of the powers of the interfering symbols, and therefore gives a rather extreme measure of it.

Let us first discuss the desired properties of $\phi(t)$ by assuming that the channel impulse response is indeed a single pulse. Nyquist pulses are a class of pulses that satisfy (10) [18]. Since $\phi(t)$ is constrained to the bandwidth available in the system, we select for our discussion $\phi(t)$ to be a raised cosine pulse of the form

$$\phi(t) = \frac{\sin(\pi t/T_s)}{\pi t/T_s} \frac{\cos \alpha \pi t/T_s}{1 - (2\alpha \pi t/T_s)^2}, \tag{12}$$

with $0 \leq \alpha \leq 1$ denoting the percent of excess bandwidth. The corresponding spectrum $\Phi(f)$ is given by

$$\Phi(f) = \begin{cases} T_s, & |f| \leq \frac{1-\alpha}{2T_s}, \\ \frac{T_s}{2}\left[1 - \sin\left[\frac{\pi}{\alpha}(f - \frac{1}{2T_s})\right]\right], & \frac{1-\alpha}{2T_s} < |f| < \frac{1+\alpha}{2T_s}, \\ 0, & |f| \geq \frac{1+\alpha}{2T_s}. \end{cases} \tag{13}$$

This pulse clearly satisfies the zero-ISI criterion in (10) and has unit power. Moreover its envelope decays as $1/t^3$. The signal bandwidth $B$ is then related to the symbol time by $B = (1 + \alpha)/T_s$.

The choice of the pulse-shaping function affects the calculation of the ISI. We expect that lower values of $\alpha$ (pulses closer to a *sinc* function) result in higher ISI, because their temporal sidelobes decay more slowly. In order to keep our comparisons fair, the performance of different channels and/or transmission schemes is analyzed using the same pulse shaping function.

Let us now shift our focus to $H_{TR}(f)$. Given our choice of the pulse shaping function $\phi(t)$, we would ideally want this to be constant over the bandwidth of interest. $H_{TR}(f)$ is the sum of matched filters $|H_m(f)|^2$ of each of the channel transfer functions from eq. 8. Even though the amplitude of $|H_m(f)|^2$ can vary randomly with frequency, the sum of $M$ such terms is expected to be nearly constant over the bandwidth if $M$ is not small (*see* Fig. 1 for illustration). Therefore, we expect the signal received at Rx given by (6) to be compressed in time, and ISI to be reduced.

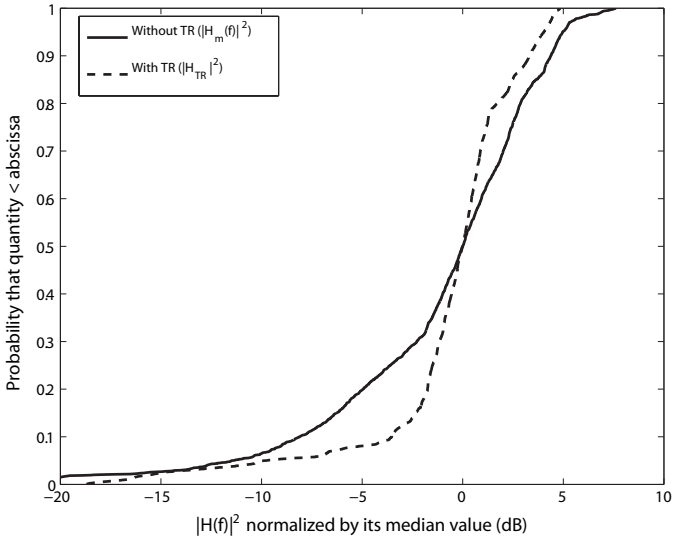


Fig. 1. The cumulative density function of the channel transfer function with and without time reversal. We have normalized each plot by its median value because the quantity of interest in terms of channel flattening is the variance around it. The plots clearly demonstrate that the equivalent channel transfer function with time reversal has smaller variance around its median value over the frequency band, which illustrates that TR results in flattening over frequency.

To investigate the quality of temporal compression, we calculate the temporal peak-to-sidelobe ratio, which is a commonly used physical performance indicator. This quantity has been used to study the effectiveness of time reversal and passive-phase conjugation for underwater acoustic communications [22]. Here, we define the temporal peak-to-sidelobe ratio using the equivalent baseband channel impulse response at the Rx, $|h_{eq,bb}(\mathbf{r}_{\text{Rx}}, t)|^2$. Let us define the time axis such that the equivalent channel impulse response achieves its maximum at $t = 0$, and let $t_{\text{sidelobe}}$ denote the time at which the power delay spread profile achieves its second largest value. We now define the temporal peak-to-sidelobe ratio to be $20\log_{10}[|h_{eq,bb}(\mathbf{r}_{\text{Rx}}, 0)|/|h_{eq,bb}(\mathbf{r}_{\text{Rx}}, t_{\text{sidelobe}})|]$. It is desirable to have as high a temporal peak-to-sidelobe ratio as possible, since that indicates good time-compression. Other measures of the temporal focusing include moments of the power-delay-profile, see *e.g.* equations (23)-(24), which attempt to capture the "tightness" of the recompression.

### C. Spatial Focusing

The formulation given above for the MISO-TR system does not reflect the spatial properties of signal propagation in the channel. To explain the spatial focusing properties of the MISO-TR system, we introduce the time harmonic Green's function $G(\mathbf{r}, \mathbf{r}'; f)$. It satisfies the Helmholtz equation

$$\Delta G + k^2 n^2(\mathbf{r}) G = -\delta(\mathbf{r} - \mathbf{r}'), \tag{14}$$

with $k = 2\pi f/c_0$ denoting the wavenumber and $c_0$ denoting the reference propagation speed. The index of refraction at position $\mathbf{r}$ is defined as $n(\mathbf{r}) = c_0/c(\mathbf{r})$. If there are random inhomogeneities in the medium, the propagation speed $c(\mathbf{r})$ fluctuates randomly.

Let $\mathbf{r}_m$ denote the spatial position of element $m$ of the Tx array and $\mathbf{r}_{\text{Rx}}$ denote the spatial position of the Rx. Using the previous notation

$$H_m(f) = G(\mathbf{r}_{\text{Rx}}, \mathbf{r}_m; f) = G(\mathbf{r}_m, \mathbf{r}_{\text{Rx}}; f). \tag{15}$$

Here, we make the assumption of perfect reciprocity; as demonstrated by Kuperman *et. al.* this degrades over time in ocean acoustics [9], [10].

The MISO-TR channel transfer function (without taking the pulse shaping into account) and the power normalization factor are given in terms of $G$ as

$$H_{\text{TR}}(\mathbf{r}, f; \mathbf{r}_{\text{Rx}}) = \sum_{m=1}^{M} G(\mathbf{r}, \mathbf{r}_m; f)\overline{G(\mathbf{r}_m, \mathbf{r}_{\text{Rx}}; f)}. \tag{16}$$

and

$$A = \left[\sum_{m=1}^{M} \int_B G(\mathbf{r}_{\text{Rx}}, \mathbf{r}_m; f)\overline{G(\mathbf{r}_m, \mathbf{r}_{\text{Rx}}; f)}\mathrm{d}f\right]^{-1/2}. \tag{17}$$

Let us consider the signal received at a location $\mathbf{r} \neq \mathbf{r}_{\text{Rx}}$ when time-reversal is performed to target a source at $\mathbf{r}_{\text{Rx}}$. We generalize (7) and obtain a space-dependent channel transfer function in the MISO-TR situation

$$H_{eq}(\mathbf{r}, f; \mathbf{r}_{\text{Rx}}) = \sqrt{P} A H_{\text{TR}}(\mathbf{r}, f; \mathbf{r}_{\text{Rx}})\overline{\Phi(f - f_0)}. \tag{18}$$

The signal sent by the Tx and received at any location $\mathbf{r}$ is

$$Y(\mathbf{r}, f; \mathbf{r}_{\text{Rx}}) = A\sqrt{P} H_{\text{TR}}(\mathbf{r}, f; \mathbf{r}_{\text{Rx}})\overline{\Phi(f - f_0)} \sum_{k=-\infty}^{\infty} \beta_k e^{i2\pi f k T_s}. \tag{19}$$

Let us assume a linear Tx array. In a homogeneous medium, $H_{\text{TR}}(\mathbf{r}, f; \mathbf{r}_{\text{Rx}})$ behaves like a *sinc* function with respect to the coordinate of $\mathbf{r} - \mathbf{r}_{\text{Rx}}$ that is parallel to the array making up the Tx [26]. For a random medium in which multipathing is significant, $H_{\text{TR}}(\mathbf{r}, f; \mathbf{r}_{\text{Rx}})$ is more tightly peaked about $\mathbf{r} = \mathbf{r}_{\text{Rx}}$. This enhanced focusing or super-resolution in TR has been analyzed by Jackson and Dowling [15]–[17]. The role that bandwidth plays in statistical stability in TR has been analyzed theoretically and numerically [4], [26]. Statistical stability occurs when the equivalent channel $h_{\text{TR}}(\mathbf{r}, t; \mathbf{r}_{\text{Rx}})$ is peaked strongly in space and time in a robust way that does not depend on the detailed features of the random medium.

To investigate the quality of spatial focusing, we define the cross-range peak-to-sidelobe ratio as our performance measure. In our 2-dimensional simulation, described in the next section, $\mathbf{r} = (r, z)$. We first compute the quantity

$$\eta(z) = \max |h^{\text{offset}}_{eq,bb}((r_{\text{Rx}}, z), t; (r_{\text{Rx}}, z_{\text{Rx}}))|^2. \tag{20}$$

This corresponds to the maximum over time of the signal at any offset location $\mathbf{r} = (r_{\text{Rx}}, z)$. Due to the spatial focusing properties of TR, we expect the function $\eta(z)$ to obtain its maximum value at $z = z_{\text{Rx}}$. Let $z = z_{\text{sidelobe}}$ denote the location of the second largest value of $\eta(z)$. We define the cross-range peak-to-sidelobe ratio to be $10\log_{10}[\eta(z_{\text{Rx}})/\eta(z_{\text{sidelobe}})]$. It is desirable to have as high a cross-range peak-to-sidelobe ratio as possible, because that would indicate tight spatial focusing.

We note that our simulation method does not have sufficient resolution in the down-range direction to compute a meaningful down-range peak-to-sidelobe ratio. However, a qualitative comparison of the behavior of the bit-error-rate in front and behind the Rx location can be found in Fig. 11.

## III. Numerical Simulations

To study the performance properties of the MISO-TR system discussed above, we simulate numerically a two dimensional waveguide channel. The motivation for this channel model comes from underwater acoustics in shallow ocean environments. Here, we do not concentrate on detailed aspects of modeling the ocean but we keep the essential features of underwater propagation to study the performance of the MISO-TR system. In particular, we focus on the role of DS·B in spatial focusing and temporal compression.

In all simulations the central frequency is $f_0 = 3.5\,\text{kHz}$ and the symbol period is $T_s = 0.57\,\text{ms}$. As the pilot signal we use a raised cosine pulse defined in (12) and (13). In Section IV we show the effect of pulse shaping by presenting the results for two values of $\alpha$, namely $\alpha = 0$ and $\alpha = 0.3$. From $T_s$ and $\alpha$, we find the bandwidth to be $B = 1.75\,\text{kHz}$ ($50\%$ of $f_0$) and $B = 2.275\,\text{kHz}$ ($65\%$ of $f_0$), respectively. The reference propagation speed is $c_0 = 1500\,\text{m/s}$. Hence, the central wavelength is $\lambda_0 = 43\,\text{cm}$.

Our simulation channel is a two dimensional, transversally periodic waveguide. The cross-range coordinate (depth) is given by $z$ and the down-range (propagation-direction) coordinate is given by $r$. The width of the waveguide is $51.2\,\text{m}$. The Rx is $1000\,\text{m}$ down-range from the Tx. The Tx is a linear array that is parallel to the cross-range coordinate. It consists of $M = 41$ elements. Adjacent elements are separated by $\lambda_0/4$. We place the origin of our coordinate system at the center of the Tx array, which is centered in the waveguide and extends from $-2\,\text{m} \le z \le 2\,\text{m}$. The Rx is located at $\mathbf{r}_{\text{Rx}} = (r_{\text{Rx}}, z_{\text{Rx}}) = (1000\,\text{m}, -10\,\text{m})$.

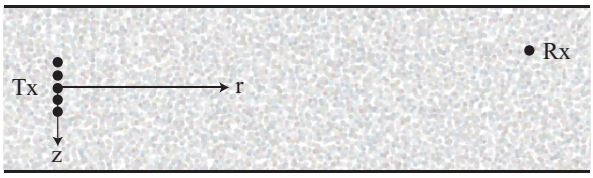


Fig. 2. The waveguide channel used for numerical simulations. The waveguide width is $51.2\,\text{m}$. The linear transmitting array Tx with $M$ elements is centered in the waveguide and spans $-2\,\text{m} \le z \le 2\,\text{m}$. The receiver Rx is located at $(r_{\text{Rx}}, z_{\text{Rx}}) = (1000\,\text{m}, -10\,\text{m})$. The waveguide contains random inhomogeneities that cause the refractive index to fluctuate randomly.

The waveguide channel has random inhomogeneities that make the refractive index vary randomly. We model this randomly varying refractive index as

$$n(\mathbf{r}) = \sqrt{1 + \sigma\mu(\mathbf{r}/\ell)}, \tag{21}$$

with $\mu$ denoting an isotropic, Gaussian correlated, random function. Realizations of $\mu(\mathbf{r})$ are computed using a random Fourier series. The correlation length is set to $\ell = 5\,\text{m}$ and the standard deviation or strength is set to $\sigma = 1\%$.

When there are no random inhomogeneities in the waveguide, we compute numerical simulation results in the frequency domain sampled at $1\,\text{Hz}$ by explicit summation of Fourier modes (*i.e.* the normal modes with respect to the cross-range coordinate). For the case in which the waveguide contains random inhomogeneities, we use the phase screen method [19]–[21]. This method ignores the weak backscattering and only propagates the forward propagating normal modes.

To control DS we introduce absorption into the waveguide channel. Absorption is modeled by applying a Gaussian filter in the vertical wave number domain. By varying the width of this filter, we vary the amount of absorption. Increasing the absorption by narrowing the filter width yields a smaller DS and hence a smaller DS·B. More than sound absorption in water, this kind of spatial filtering models reflection losses at the waveguide boundaries. Details on the implementation of absorption in our simulations can be found in the appendix.

## IV. Simulation Results

### A. Estimating DS·B

We show below that the key system parameter throughout our discussion is the DS for a given system bandwidth B, and therefore we compute the dimensionless product DS·B. To estimate the delay spread (DS) of the channel, we first estimate the average power delay profile $pdp(t)$ by averaging over the signals recorded by each of the elements in the transmitter:

$$pdp(t) = \frac{1}{M}\sum_{m=1}^{M} |s_m(t)|^2. \tag{22}$$

We compute the DS as the centralized second moment of the average power delay profile:

$$\text{DS} = \left[\int (t-\bar{t})^2 pdp(t)\mathrm{d}t \Big/ \int pdp(t)\mathrm{d}t\right]^{1/2}, \tag{23}$$

with

$$\bar{t} = \int t\,pdp(t)\mathrm{d}t \Big/ \int pdp(t)\mathrm{d}t. \tag{24}$$

In Fig. 3 we plot the amplitude of the acoustic field induced by the pilot signal at the Tx plane as a function of time and cross-range in a waveguide, with and without random inhomogeneities. In the figure, we have also indicated the extent of the Tx array. The Rx is $1\,\text{km}$ down-range from the Tx and its cross-range coordinate is $-10\,\text{m}$. The time axis is shifted so that $t = 0$ corresponds to the "ballistic" (line of sight) arrival time.

Fig. 3(a) shows the results for a waveguide containing no random inhomogeneities. For that case, the regular pattern observed corresponds to reflections off the waveguide walls. In contrast, Fig. 3(b) shows the result for a waveguide containing random inhomogeneities. There is still a dominant regular pattern due to reflections from the boundaries as seen from the comparison with Fig. 3(a). However, this signal is distorted due to multiple scattering in the channel, in the sense that waves

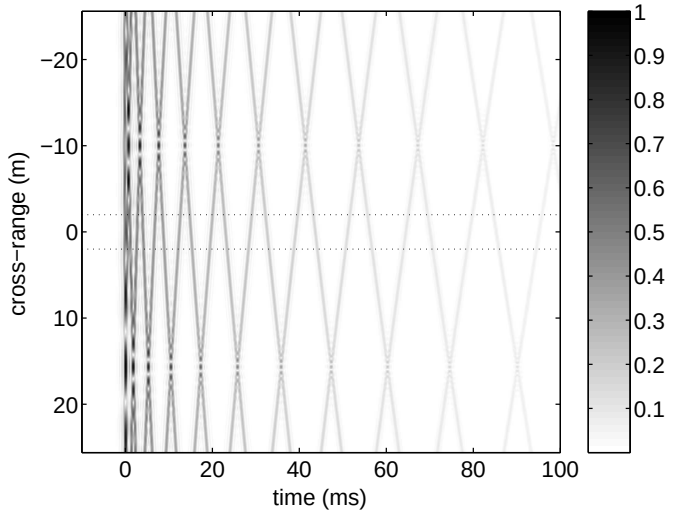


(a) without random inhomogeneities

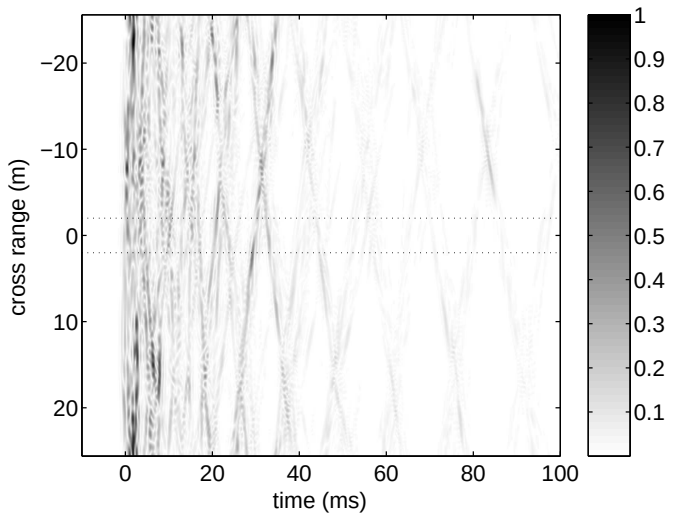


(b) with random inhomogeneities

Fig. 3. Time traces of the amplitude recorded across the Tx plane due to the pilot signal for the case in which DS·B $\approx 20$.

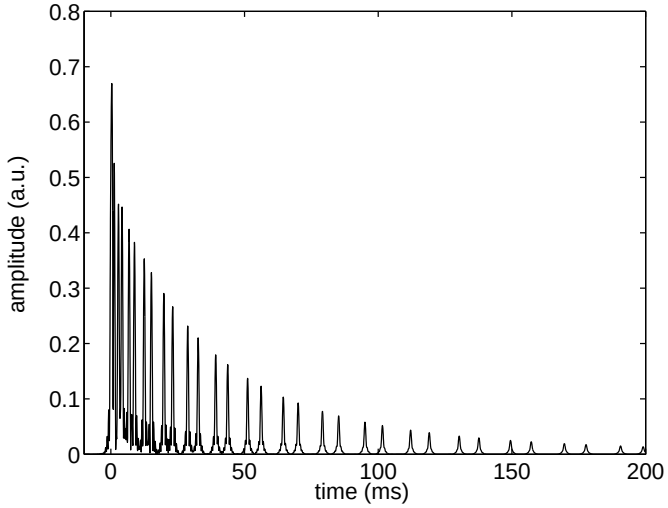


(a) without random inhomogeneities

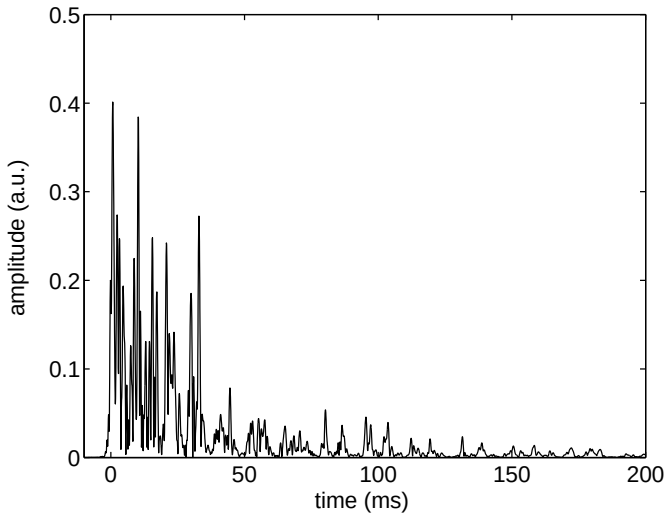


(b) with random inhomogeneities

Fig. 4. Time traces of the amplitude recorded at the center of the Tx array due to the pilot signal for the case in which DS·B $\approx 32$.

resulting from the same order reflections off the boundaries do not arrive at linearly delayed times at the various Tx array elements.

In the situation shown, DS·B $\approx 32$. The DS·B is approximately the same both with and without inhomogeneities, *i.e.* for both simulations shown in Fig. 3, because the path arrival times are dominated by the multiple reflections on the boundaries of the waveguide and not the random inhomogeneities.

Let us look in more detail at the time traces of the baseband received signal at the center element of the Tx array. Fig. 4(a) shows the results for a waveguide containing no random inhomogeneities. Fig. 4(b) shows the result for a waveguide containing random inhomogeneities. We observe that the introduction of random inhomogeneities changes the amplitudes of the reflected paths and spreads their arrival times around the nominal arrival times.

We now investigate the ramifications of this additional scattering in the channel on time reversal in terms of spatial focusing and temporal compression.

### *B. Illustration of spatial focusing and temporal compression*

We examine the focusing in space and compression in time around the Rx resulting from the application of time reversal by the elements of the Tx for the same propagation scenarios as before. Our objective is to illustrate how the results differ in waveguides with and without random inhomogeneities.

Fig. 5 shows simulation results of the amplitude of the acoustic field on the Rx plane after time reversal processing at the Tx. Here, the time axis is shifted so that $t = 0$ corresponds to the time of arrival of the peak signal at the Rx. The equivalent channel impulse response at locations off the target Rx has been calculated from (18).

Fig. 5(a) corresponds to the waveguide containing no random inhomogeneities and Fig. 5(b) corresponds to the waveguide containing random inhomogeneities. There is a sharp focusing in space and a tight compression in time for both

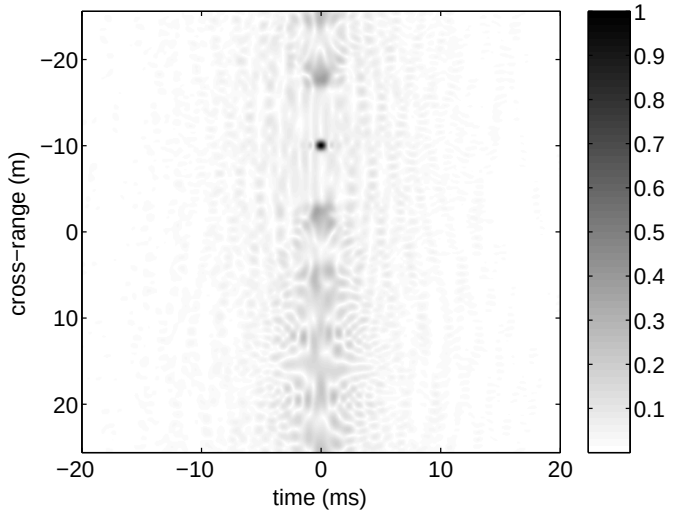


(a) without random inhomogeneities

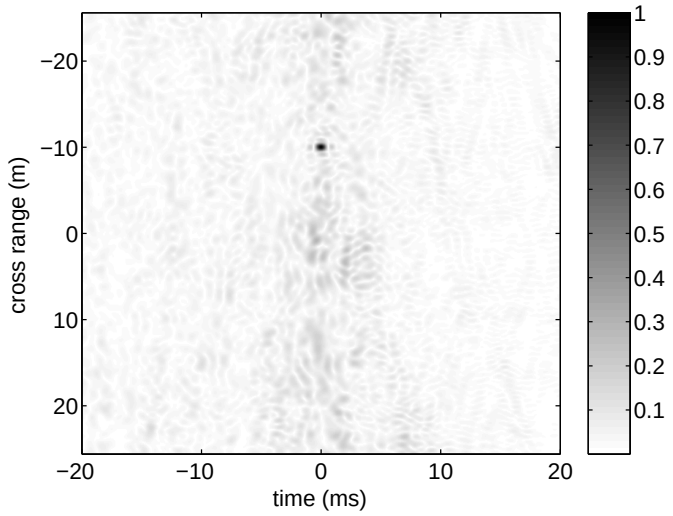


(b) with random inhomogeneities

Fig. 5. Time traces of the amplitude recorded across the Rx-plane due to the pilot signal for the case in which DS·B $\approx 20$. Each signal is normalized to its peak amplitude.

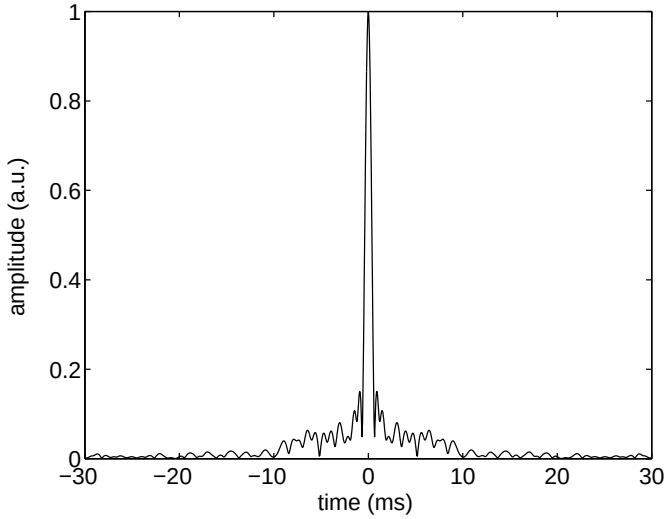


(a) without random inhomogeneities

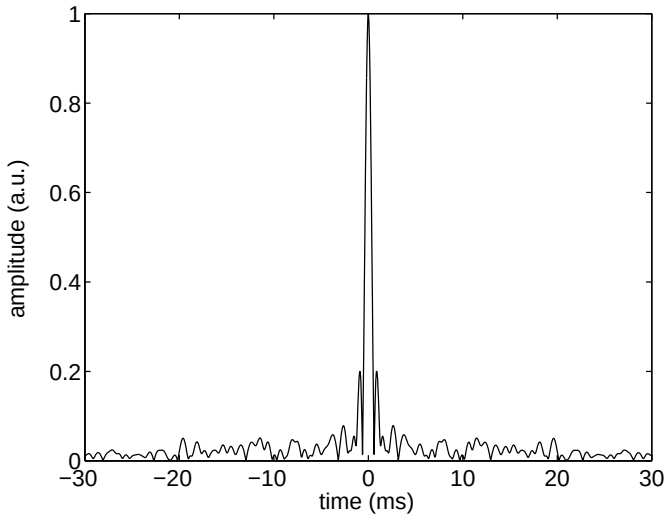


(b) with random inhomogeneities

Fig. 6. Time traces of the amplitude of the baseband equivalent channel impulse response at the Rx for the case in which DS·B $\approx 32$.

cases around the Rx. For the waveguide containing random inhomogeneities, the acoustic energy away from the Rx in space and time is smaller than the corresponding result for the waveguide with no inhomogeneities. This is due to the additional angular diversity introduced by scattering from the inhomogeneities.

Let us look in more detail at the time traces of the received signal after time reversal for the same situation as the one shown in Fig. 4. Fig. 6(a) shows the results for a waveguide containing no random inhomogeneities. Fig. 6(b) shows the result for a waveguide containing random inhomogeneities. In both cases we have normalized the peak signal to 1. We observe that both curves show pulses that appear to be more tightly compressed in time.

### *C. Dependence of spatial focusing and temporal compression on DS·B*

We now illustrate how the spatial and temporal focusing results depend on the DS·B. To do that, we keep the same geometric configuration and bandwidth, and we vary the absorption so as to have a varying DS·B product.

Fig. 7 shows the cross-range peak-to-sidelobe ratio as a function of DS·B. The solid curves are for the waveguide containing no random inhomogeneities and the dashed curves are for the waveguide containing random inhomogeneities. The results are shown for both $\alpha = 0$ and $\alpha = 0.3$. In Fig. 7 we observe the increase of the peak-to-sidelobe ratio as the DS·B increases. Hence, the quality of spatial focusing, according to the peak-to-sidelobe ratio, increases with DS·B. For the waveguide containing random inhomogeneities, we observe a nearly $3\,$dB improvement in the cross-range peak-to-sidelobe ratio in comparison with the waveguide with no inhomogeneities. These results demonstrate that the scattering

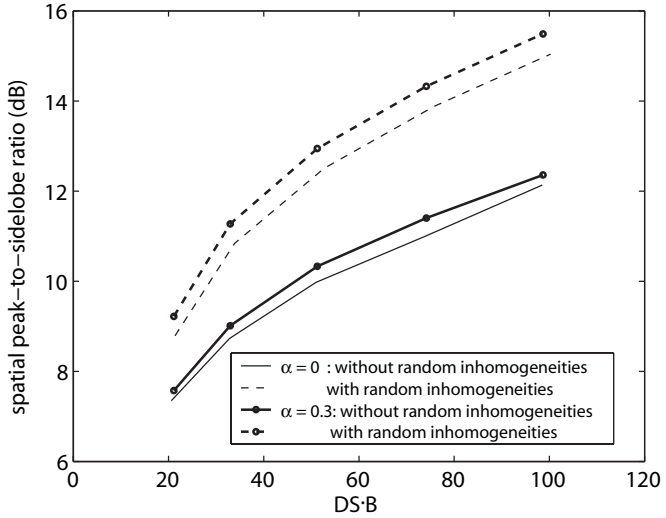


Fig. 7. The cross-range peak-to-sidelobe ratio as a function of DS·B for (a) $\alpha = 0$, (b) $\alpha = 0.3$. The solid curve is for the waveguide channel with no random inhomogeneities. The dashed curved is for the waveguide with random inhomogeneities.

due to random inhomogeneities yields an enhancement in spatial focusing. We also observe that the spatial focusing results are not influenced by our choice of $\alpha$.

To investigate the quality of temporal compression, we study first the temporal peak-to-sidelobe ratio as defined in Section II.

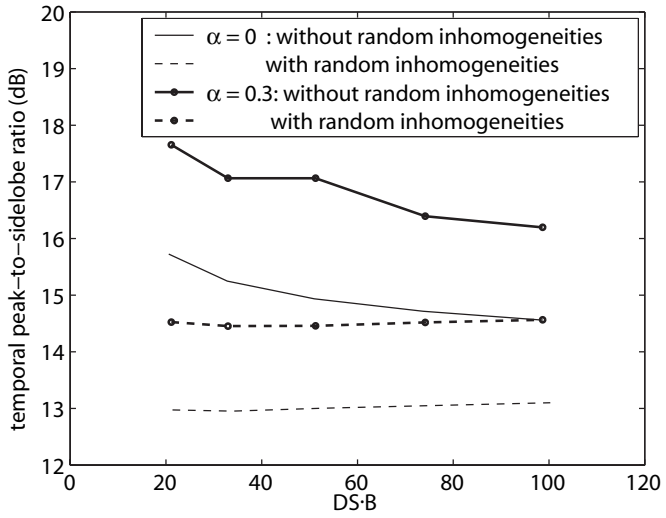


Fig. 8. The temporal peak-to-sidelobe ratio as a function of DS·B. The solid curve is for the waveguide channel with no random inhomogeneities. The dashed curved is for the waveguide with random inhomogeneities.

In Fig. 8, we plot the temporal peak-to-sidelobe ratio as a function of DS·B. The solid curves are for the waveguide containing no random inhomogeneities. The dashed curves are for the waveguide containing random inhomogeneities. The results are shown for both $\alpha = 0$ and $\alpha = 0.3$. Fig. 8 shows the remarkable temporal compression properties of time reversed signals. For both situations (with and without random inhomogeneities), the temporal peak-to-sidelobe ratio is at least 13 dB for all the values of DS·B values studied here.

The results for the channel with no random inhomogeneities show a higher (better) temporal peak-to-sidelobe ratio than those for the channel with random inhomogeneities. In particular, we observe a difference between the two cases of approximately 2 dB. We have observed this difference over several realizations of the random inhomogeneities. Moreover, the temporal peak-to-sidelobe ratio does not vary significantly with respect to DS·B in a waveguide with random inhomogeneities, whereas it reduces for a deterministic waveguide. Although TR recompresses the signal in a temporal peak-to-sidelobe sense, this improves with DS·B only in a waveguide with random inhomogeneities. For the waveguide without random inhomogeneities, the temporal peak-to-sidelobe ratio decreases with increasing DS·B.

Here we observe that pulses with higher excess bandwidth (higher percent excess bandwidth $\alpha$) have, as expected, better performance in terms of temporal compression.

One of the main results of this paper can be drawn from the comparison of Fig. 8 and Fig. 7. This shows that scattering due to random inhomogeneities in the medium adds only angular diversity. The increase in angular diversity yields more pronounced spatial focusing. However, it does not improve temporal compression. Indeed it is made worse. In the case of no random inhomogenities, the increase in DS·B also increases spatial focusing, but decreases temporal compression.

### *D. ISI results*

For a channel with large DS·B, ISI is inevitable with or without TR. If there is ISI, the Rx must equalize this signal prior to demodulating it in order to recover the bitstream sent by the Tx. For the MISO-TR system we have shown using numerical simulations that signals compress temporally. The temporal compression indicates that TR may indeed reduce the ISI in the channel.

We examine ISI for this MISO-TR system as a function of DS·B. We would like the ISI to be as low as possible.

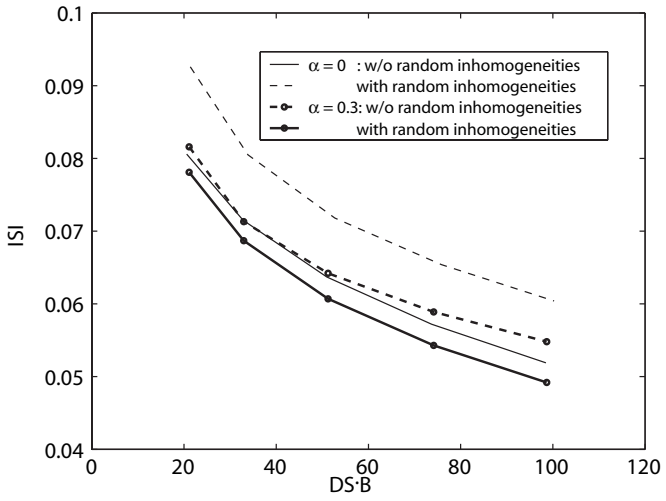


Fig. 9. The intersymbol interference as a function of DS·B. The solid curve is for the waveguide channel with no random inhomogeneities. The dashed curved is for the waveguide with random inhomogeneities.

In Fig. 9 we plot the ISI as a function of DS·B. The solid curves are for the waveguide channel containing no random inhomogeneities. The dashed curves are for the waveguide containing random inhomogeneities. The results are shown for both $\alpha = 0$ and $\alpha = 0.3$. Clearly, the application of TR reduces the ISI, and the reduction increases as DS·B increases. Moreover the ISI is higher in a waveguide with random inhomogeneities than in a waveguide without random inhomogeneities for the same DS·B.

The comparison of Fig. 8 and Fig. 9 can help us draw some important conclusions. Even though Fig. 8 showed that TR yields signals that are compressed in time, Fig. 9 shows that there remains ISI in the channel because $H_{TR}(f)$ is not flat over the bandwidth of interest and the zeros of $\phi(t)$ at the multiples of the symbol time are not preserved. The ISI results for the waveguide containing random inhomogeneities are larger than for the one without random inhomogeneities. This difference is consistent with the temporal peak-to-sidelobe ratio results shown in Fig. 8 in the sense that the performance is better in a waveguide without random inhomogeneities. However Fig. 9 shows that ISI, which is a metric more important for communications than the temporal peak-to-sidelobe ratio, reduces as DS·B increases for waveguides both with and without inhomogeneities. This is something that we cannot observe by looking at Fig. 8.

Again we observe that pulses with higher excess bandwidth (higher percent excess bandwidth $\alpha$) have, as expected, better performance in terms of temporal compression.

Arguably, ISI $< 0.1$ is not significant enough to affect detection. However, equalization would still be needed at the Rx prior to demodulation, especially in the case of finite receiver noise and for the case of higher order modulations.

These simulations have been expressed for the high signal-to-noise limit, *i.e.* we have assumed that the transmitters know the original channel impulse responses perfectly. In reality though, this channel state information will be contaminated by instrument noise during the channel estimation stage of the time-reversal process. In that case we expect to see a deterioration of the ISI. However that analysis is beyond the scope of this paper.

Finally, in our calculations, we have assumed that the MISO-TR system operates at maximum spectral efficiency. In other words, consecutive symbols are separated by exactly one symbol period. The overall ISI can be reduced by rate back-off in which subsequent symbols are delayed by more than one symbol period at the expense of reduced transmission rate. Similar conclusions have been made regarding MISO-TR for indoor wireless [23], [24].

### *E. Signal detection at off-target locations*

Although TR yields temporally compressed signals that help to reduce ISI in the channel, the main value added in using TR is spatial focusing. Thanks to spatial focusing, a MISO-TR system can be used to transmit signals clearly to the desired Rx, but these cannot be reliably decoded anywhere else using the same type of single-receiver technology. Hence, MISO-TR exhibits some LPI capability in this limited sense.

To show the LPI properties of the MISO-TR system, we show in Fig. 10 the sampled received signal, as well as the corresponding bit error rates (BER), at (a) $z = z_{\text{Rx}}$, (b) $z = z_{\text{Rx}} + \lambda$, and (c) $z = z_{\text{Rx}} + 2\lambda$, assuming that 1000 consecutive symbols selected from a BPSK constellation have been transmitted through the waveguide channel containing random inhomogeneities (DS·B $\approx 50$). For each plot, the power of the received symbol is normalized by the value of the equivalent channel impulse response at $t = 0$, so as to map the received signal to the originally transmitted BPSK symbols $\pm 1$. A hard decoder compares the sampled symbol with 0, and determines that $+1$ had been transmitted if the sampled signal is greater than 0, and $-1$ otherwise. An error occurs when the hard detector decision is different from the transmitted signal. This can happen if the ISI (and possibly the noise in the finite signal to noise ratio scenario) is high enough for the received signal to be in the wrong decision region.

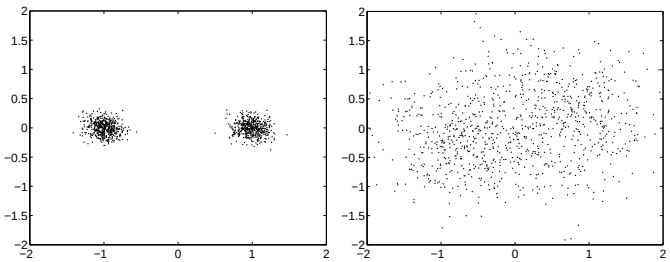

(a) $r = r_{\text{Rx}}$, BER $= 0$ (b) $z = z_{\text{Rx}} + \lambda$, BER $= 0.22$

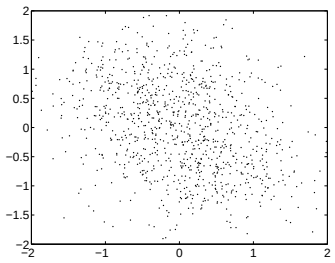

(c) $z = z_{\text{Rx}} + 2\lambda$, BER $= 0.61$

Fig. 10. BPSK constellation plots for 1000 bits transmitted through the waveguide channel with DS·B $\approx 50$ containing random inhomogeneities. These constellation plots were obtained from the signal $y(r_{\text{Rx}}, z, t)$ with (a) $z = z_{\text{Rx}}$, BER $= 0$, (b) $z = z_{\text{Rx}} + \lambda$, BER $= 0.22$ and (c) $z = z_{\text{Rx}} + 2\lambda$, BER $= 0.61$.

We observe in Fig. 10(a) that the symbols are clearly distinguishable at the Rx location. There is ISI (the sampled symbols are spread about $\pm 1$ and are not identically $\pm 1$), consistent with the results shown in Fig. 9. Therefore, one cannot use an arbitrarily large constellation effectively due to this ISI. In Fig. 10(b) we see that symbols are barely distinguishable at best even though the signal is received at only one wavelength away in cross-range from Rx. This situation becomes more extreme at two wavelengths away in the cross-range from the Rx as shown in Fig. 10(c). Therefore, our numerical simulations confirm that this MISO-TR system has a limited LPI capability in the sense that, when no equalization is utilized at the receiver side, only the intended Rx can clearly distinguish the symbols sent by the Tx.

The results shown above are for the case where $\alpha = 0.3$.

Similar performance is observed when $\alpha = 0$.

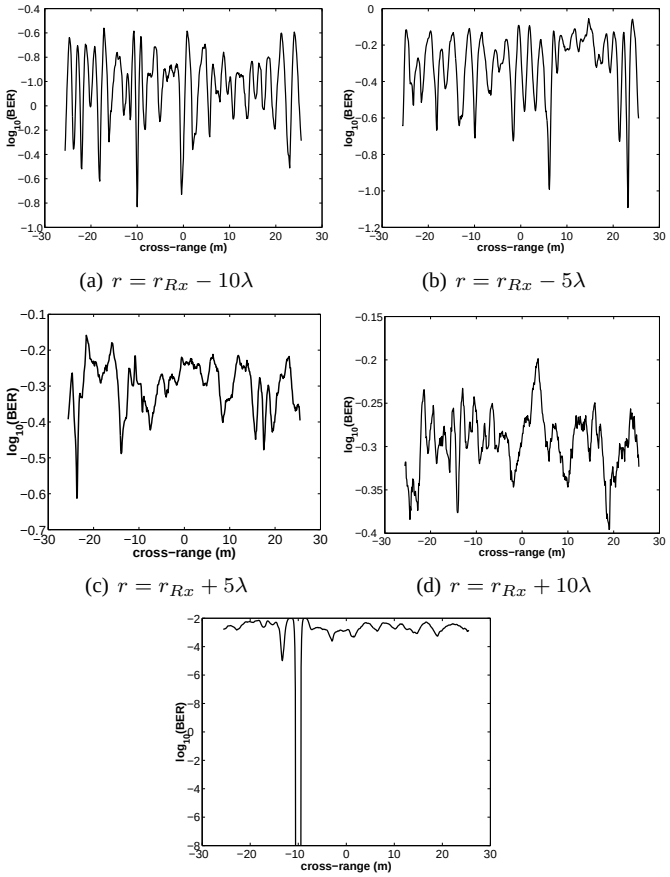


(a) $r = r_{Rx} - 10\lambda$ (b) $r = r_{Rx} - 5\lambda$

(c) $r = r_{Rx} + 5\lambda$ (d) $r = r_{Rx} + 10\lambda$

(e) $r = r_{Rx}$ (reference)

Fig. 11. The bit-error-rate as a function of cross-range ($z$), presented at five different down-range ($r$) locations: offsets of $\{-10\lambda, -5\lambda, +5\lambda, +10\lambda\}$ as well as in the correct focal location $r_{Rx}$.

In order to generalize this result in the down-range, Fig. 11 shows the bit error rate (BER) as a function of the waveguide cross-section at various down-ranges $r$. For these simulations DS·B≈30. These estimates are for one realization of the random inhomogeneities, but similar results are observed for all other realizations. Clearly at ranges other than that of the intended receiver, the BER is prohibitively high.

## V. Pre-equalizing the channel

Simulation results in the previous sections show that the pure time reversal scheme does not yield perfect ISI suppression. Suppose that the signal to be transmitted is pre-filtered by a filter common to all the Tx elements before it goes through the time reversal filters at each Tx element. Can such a filter be designed to eliminate ISI? We investigate this question by attempting a transmit-side zero-forcing to pre-equalize the channel and thereby remove ISI.

For illustration of principle we are going to assume that the percent excess bandwidth of the pulse-shaping function is $\alpha = 0$, but the result can without loss of generality be applied for arbitrary pulse shaping.

To do this we extend (7) by allowing the scaling $A$ to depend on frequency, *i.e.* we introduce a filter $A(f)$ that is applied to the signal $X(f)$ before it goes through the time reversal filters at the Tx elements. We denote the resulting equivalent channel transfer function as $H_{\text{eq}}^{\text{ZF}}(f)$:

$$H_{\text{eq}}^{\text{ZF}}(f) = A(f)\overline{\Phi(f - f_0)}H_{TR}(f), \tag{25}$$

and we select

$$A(f) = \Gamma(f) \Big/ \left[\int_B |\Gamma(f)|^2 H_{TR}(f)\mathrm{d}f\right]^{1/2} \tag{26}$$

where

$$\Gamma(f) = \begin{cases} (H_{TR}(f))^{-1}, & |H_{TR}(f)|^{-1} > \delta, \\ 1/\delta, & |H_{TR}(f)|^{-1} \leq \delta, \end{cases} \tag{27}$$

with $\delta$ denoting a prescribed threshold value. Suppose that $\gamma(f)$ is non-zero for all $f \in B$ and $\delta = 0$. For that case, (25) reduces to a perfectly flat channel. Hence, the signal recorded at the Rx should be free of ISI. However, it is not known if this generalization of time reversal compromises the quality of spatial focusing. We investigate these issues using numerical simulations.

### A. Illustration of ZF effects

Fig. 12 shows the equivalent baseband channel impulse response with and without ZF prefiltering at the transmitter for a waveguide with and without random inhomogeneities. The time axis has been shifted so that $t = 0$ corresponds to the time of arrival of the strongest signal. We observe that although the pulses both with and without ZF are compressed in time, the introduction of ZF preserves the zeros of the equivalent baseband channel impulse response at the integer multiples of the symbol time. This is not true for the equivalent channel impulse response from (7).

Moreover, all signals in Fig. 12 have been generated after having normalized the transmit power to 1. We observe a significant decrease in peak power if ZF pre-equalization is used. Indeed, it has been shown that time reversal as in (7) is the scheme that delivers the highest peak power at the Rx under a constant transmit power constraint [25].

In Fig. 13 we show the peak power of the equivalent channel impulse response as a function of cross-range distance from the Rx. We again observe that the peak power of the equivalent channel impulse response with ZF pre- equalization is lower than the equivalent channel impulse response from (7), however it only appears to be offset relative to that and not distorted.

### B. Dependence of spatial focusing and ISI on DS·B

The application of a zero-forcing pre-equalizer eliminates the ISI from the signal.

In Fig. 14 we show the cross-range peak to sidelobe ratio as a function of DS·B for waveguides with and without inhomogeneities. The solid curves correspond to the standard time-reversal system and the dashed curves are for the transmit-side zero-forcing system. According to these numerical simulation results, we observe that transmit side zero-forcing does not compromise the relative spatial focusing of time reversal

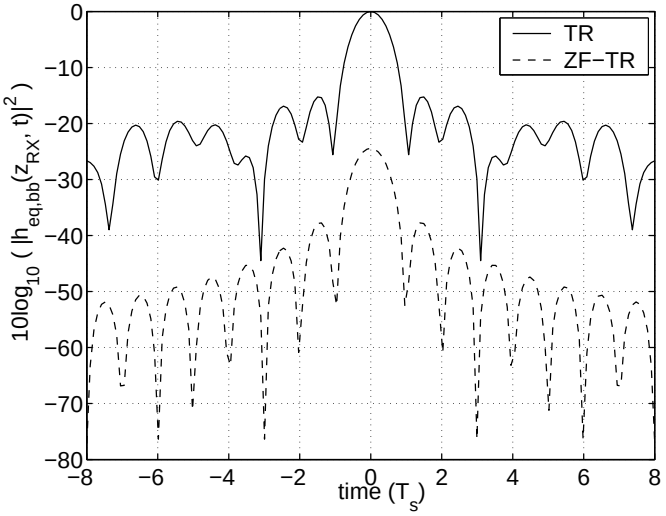


(a) without random inhomogeneities

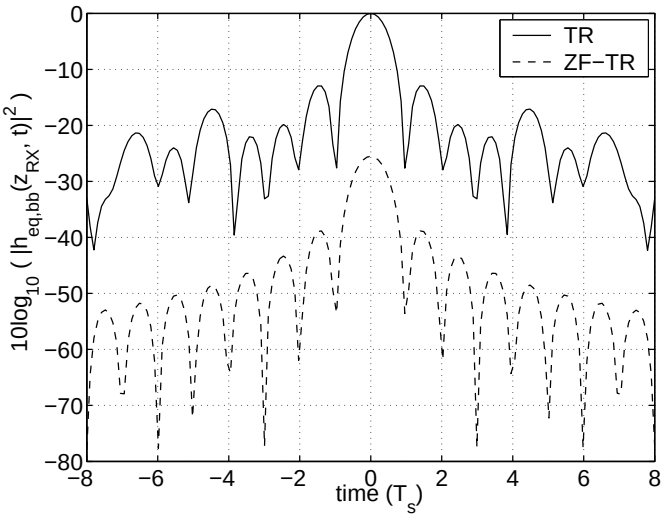


(b) with random inhomogeneities

Fig. 12. Time traces of the power of the baseband equivalent channel impulse response at the Rx with and without ZF for the case in which DS·B $\approx 32$.

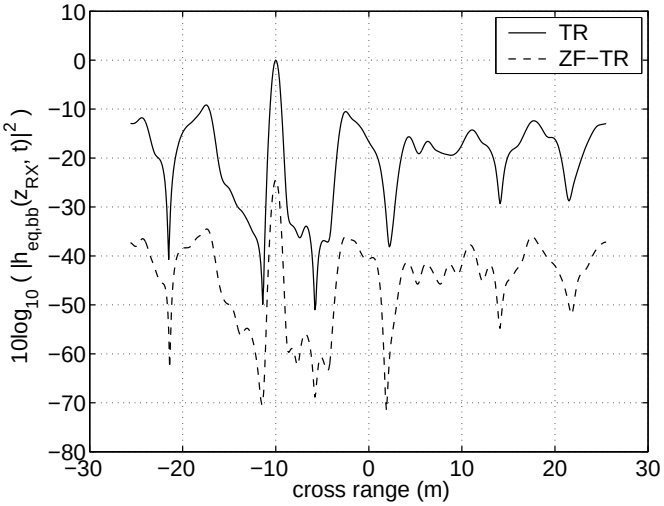


(a) without random inhomogeneities

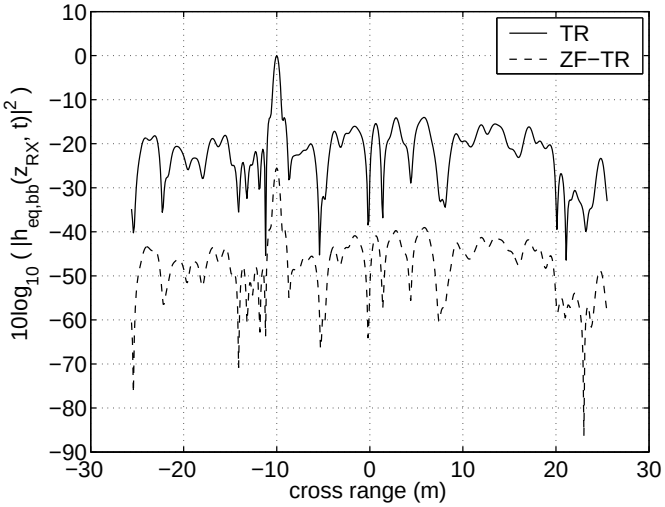


(b) with random inhomogeneities

Fig. 13. Traces of the peak power of the baseband equivalent channel impulse response around the Rx with and without ZF for the case in which DS·B $\approx 32$.

significantly. Therefore the cost of using transmit-side zero-forcing compared with standard time reversal is only increased complexity at the Tx. As shown earlier, the spatial focusing is better in a waveguide with random inhomogeneities.

Fig. 12 showed that the introduction of the ZF pre-equalization reduces the peak power at the Rx. In Fig. 15 we show the ratio of the peak powers with and without ZF $\eta_{ZF\text{-}TR}(0)/\eta_{TR}(0)$ in a waveguide with random inhomogeneities. Clearly ZF pre-filtering reduces the peak power at the intended receiver. The power penalty of applying a ZF pre-equalizer increases as the DS·B decreases. Low DS·B is due to high absorption. In that case, mainly low order reflections dominate (small angles of arrival) and the signals on all the elements of the transmit array are similar for all delays. Therefore there is no significant averaging benefit from the summation over the transmit elements: $H_{TR}$ is approximately as frequency selective as each of the $H_m(f)$, and the ZF prefilter equalizes the channel at the expense of peak power.

### C. Illustration of LPI

We want to demonstrate that the introduction of the ZF does not affect adversely the LPI properties of TR in the sense that the signal suffers a significant loss of coherence away from the intended receiver. Fig. 16 shows the constellation plots for this modified system in a waveguide with random inhomogeneities. All parameters are the same as in Fig. 10(b). We observe nearly zero ISI at the Rx, but for any location away from the Rx, the symbols cannot be successfully decoded.

Similar results are observed in a waveguide without random inhomogeneities.

## VI. Conclusions

We have studied the spatial focusing and temporal compression properties of a MISO-TR system. Using numerical simulations of acoustic wave propagation in a two dimensional waveguide, we have investigated the effect on both spatial focusing and temporal compression of the delay spread for

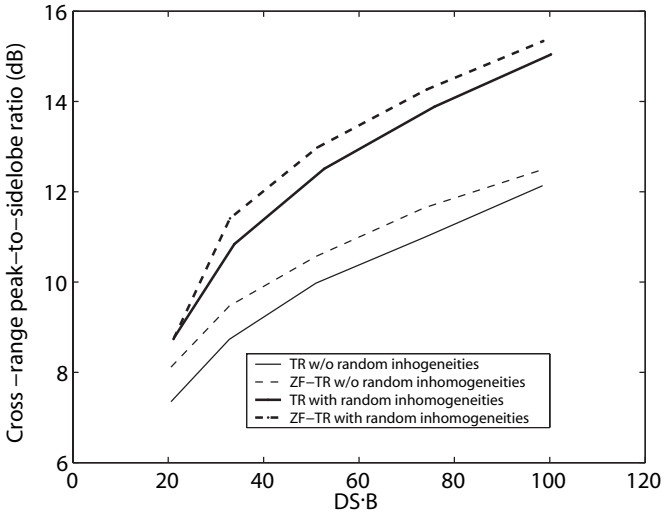


Fig. 14. Cross-range peak to sidelobe ratio with and without ZF pre-equalization versus DS·B (a) in a waveguide without random inhomogeneities, (b) in a waveguide with random inhomogeneities. The solid curve is for the case with standard time reversal and the dashed curved is for the case with transmit-side zero-forcing.

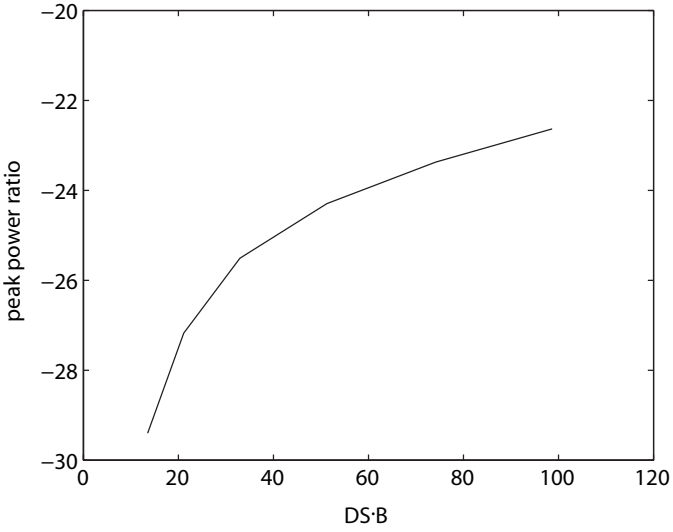


Fig. 15. The peak power ratio $\eta_{ZF\text{-}TR}(0)/\eta_{TR}(0)$ as a function of DS·B in a waveguide with random inhomogeneities (the result is shown in dB.)

a given system bandwidth. Moreover we repeated the calculations for deterministic and random waveguides. As our performance indicators, we used both physical and communications related metrics.

We found that the physical metrics for TR do not reflect correctly the communications metrics as the delay spread increases, especially in channels with random inhomogeneities.

Multiple scattering in the channel due to random inhomogeneities adds angular diversity thereby enhancing the spatial focusing. However, this multiple scattering degrades the temporal compression and increases ISI. The existence of ISI indicates that equalization is needed before signal demodulation despite the fact that the signal has been compressed temporally.

We have found that, in line with expectation, time-reversal

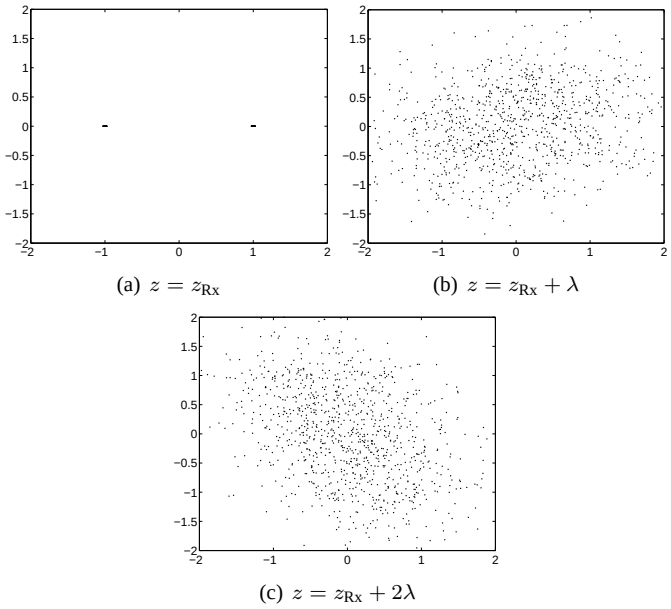


Fig. 16. The same as Fig. 10, but using the transmit-side zero-forcing pre-filter. These constellation plots were obtained from the signal $y(r_{\mathrm{Rx}}, z, t)$ with (a)$z = z_{\mathrm{Rx}}, \mathrm{BER} = 0$, (b) $z = z_{\mathrm{Rx}} + \lambda, \mathrm{BER} = 0.17$ and (c) $z = z_{\mathrm{Rx}} + 2\lambda, \mathrm{BER} = 0.65$.

decreases the ISI. However, with increasing randomness in the environment, the ISI is higher, *even though* the spatial focusing becomes tighter.

The spatial focusing properties indicate that this MISO-TR system can transmit with LPI as indicated by a dramatic increase in the BER away from the Rx for the case when no equalization is used at the Rx. For example, our simulations show that one can distinguish BPSK symbols clearly at the Rx, but cannot reliably decode them at a location one wavelength away from Rx. This rapid loss of coherence may contribute to the overall security in future communication systems. The deployment of superior technologies, or extreme luck on the part of the eavesdropper can defeat this "physical security" which therefore cannot be relied on exclusively.

We have proposed a transmit-side zero-forcing pre-filter. By increasing the complexity of the signal processing at the Tx, we have shown that this modified system mitigates nearly all channel ISI. This happens at the expense of peak power at the receiver. Most importantly, this additional processing at the transmitter does not adversely affect the spatial focusing. Therefore, this system has LPI without any ISI at the desired Rx.

## ACKNOWLEDGMENT

The work of A. D. Kim P. Kyritsi and G. Papanicolaou were supported partially by grants AFOSR: F49620-01-1-0465 and ONR: N0001402-1-0088. The work of P. Blomgren was supported partially by grant ONR: N0001402-1-0088.

## APPENDIX: ABSORPTION MODEL

Suppose the acoustic field $u(r_1, z; f)$ over the plane $r = r_1$ is known. We seek the field $u(r_1 + \delta r, z; f)$ in terms of it. We

represent $u(r_1, z; f)$ in terms of its Fourier series

$$u(r_1, z; f) = \sum_{j=-\infty}^{\infty} u_j(r_1; f) e^{i\zeta_j z}, \tag{28}$$

with

$$\zeta_j = 2\pi j / Z_0, \tag{29}$$

and $Z_0$ denoting the width of the waveguide. To propagate this field to $r_2 = r_1 + \delta r$ in the absence of absorption, we compute

$$u(r_2, z; f) = \sum_{j=-\infty}^{\infty} u_j(r_2; f) e^{i\zeta_j z}, \tag{30}$$

with $k = 2\pi f / c_0$, and (*see e.g.* [20] or [21])

$$u_j(r_2; f) = u_j(r_1; f) e^{ik\delta r \sqrt{1-\zeta_j^2/k^2}}. \tag{31}$$

We model absorption by applying a Gaussian filter on the Fourier modes defined in (31). Hence, we replace (30) by

$$u(r_2, z; f) = \sum_{j=-\infty}^{\infty} v_j(r_2; f) e^{i\zeta_j z}, \tag{32}$$

with

$$v_j(r_2; f) = u_j(r_1; f) e^{ik\delta r \sqrt{1-\zeta_j^2/k^2}} e^{-\zeta_j^2/w^2}. \tag{33}$$

Here, $w$ denotes the width of the Gaussian filter. For our simulations, $20 \leq w \leq 80$ yielded approximately $20 \leq$ DS·B $\leq 100$.

## REFERENCES


[1] M. Fink, "Time reversed acoustics," *Physics Today*, March, pp. 33-40, 1997.

[2] M. Fink, "Time-reversed acoustics," *Scientific American*, November, pp. 91-97, 1999.

[3] M. Fink, D. Cassereau, A. Derode, C. Prada, P. Roux, M. Tanter, J-L. Thomas and F. Wu, "Time-reversed acoustics," *Reports on Progress in Physics*, vol. 63, pp. 1933-1995, 2000.

[4] P. Blomgren, G. Papanicolaou and H. Zhao, "Super-resolution in time-reversal acoustics," *J. Acoust. Soc. Am*, vol. 111, pp. 230-248, 2002.

[5] W. A. Kuperman, W. S. Hodgkiss, H. C. Song, T. Akal, C. Ferla, and D. R. Jackson, "Phase conjugation in the ocean: Experimental demonstration of a time reversal mirror," *J. Acoust. Soc. Am.*, vol. 103, pp. 25-40, 1998.

[6] W. S. Hodgkiss, H. C. Song, W. A. Kuperman, T. Akal, C. Ferla and D. R. Jackson, "A long-range and variable focus phase-conjugation experiment in shallow water," *J. Acoust. Soc. Am.*, vol. 105, pp. 1597-1604, 1999.

[7] S. Kim, G. Edelmann, W. S. Hodgkiss, W. A. Kuperman, H. C. Song, and T. Akal, "Spatial resolution of time reversal array in shallow water," *J. Acoust. Soc. Am.*, vol. 110, pp. 820-829, 2001.

[8] G. Edelmann, T. Akal, W. S. Hodgkiss, S. Kim, W. A. Kuperman, H. C. Song, "An initial demonstration underwater acoustic communication using time reversal," *IEEE J. of Oceanic Eng.*, vol. 27, pp. 602-609, 2002.

[9] S. Kim, W. A. Kuperman, W. S. Hodgkiss, H. C. Song, G. Edelmann, and T. Akal, "Robust time reversal focusing in the ocean," *J. Acoust. Soc. Am.*, vol. 114, pp. 145-157, 2003.

[10] P. Roux, W. A. Kuperman, W. S. Hodgkiss, H. C. Song, T. Akal, and M. Stevenson, "A nonreciprocal implementation of time reversal in the ocean," *J. Acoust. Soc. Am.*, vol. 116, pp.1009-1015, 2004.

[11] D. Rouseff, D. R. Jackson, W. L. J. Fox, C. D. Jones, J. A. Ritcey and D. R. Dowling, "Underwater acoustic communication by passive-phase conjugation: theory and experimental results," *IEEE J. Oceanic Eng.*, vol. 26, pp. 821-831, 2001.

[12] D. Rouseff, "Intersymbol interference in underwater acoustic communications using time-reversal signal processing," submitted to *J. Acoust. Soc. Am.*, 2004.

[13] C. Oestges, A. D. Kim, G. Papanicolaou, A. J. Paulraj, "Characterization of space-time focusing in time-reversed random fields," *IEEE Trans. Antennas Propagat.*, vol. 53, no 1, part 2, pp. 283-293, Jan. 2005.

[14] P. Kyritsi, G. Papanicolaou, P. Eggers and A. Opera, "MISO time reversal and delay spread compression for FWA channels at 5 GHz," *Antennas and Wireless Propagation Letters* vol. 3, pp. 96-99, 2004.

[15] D. R. Dowling and D. R. Jackson, "Phase conjugation in underwater acoustics," *J. Acoust. Soc. Am.*, vol. 89, pp. 171-181, 1990.

[16] D. R. Dowling and D. R. Jackson, "Narrow-band performance of phase-conjugate arrays in dynamic random media," *J. Acoust. Soc. Am.*, vol. 91, pp. 3257-3277, 1992.

[17] D. R. Dowling, "Acoustic pulse compression using passive phase-conjugate processing," *J. Acoust. Soc. Am.*, vol. 95, pp. 1450-1458, 1994.

[18] J. G. Proakis, *Digital Communications* 4th ed. McGraw-Hill, New York, 2001.

[19] J. M. Martin and S. M. Flatté, "Intensity Images and Statistics from Numerical Simulation of Wave Propagation in 3D Random Media," Appl. Optics, **27** 2111–2126 (1988).

[20] M. D. Collins, "Higher-order Padé approximations for accurate and stable elastic parabolic equations with applications to interface wave propagation," *J. Acoust. Soc. Am.*, vol. 89, pp. 1050-1057, 1991.

[21] M. D. Collins, "Generalization of the split-step Padé solution," *J. Acoust. Soc. Am.*, vol. 96, pp. 382-385, 1994.

[22] T. C. Yang, "Temporal resolutions of time-reversal and passive-phase conjugation for underwater acoustic communications," *IEEE J. Oceanic Eng.*, vol. 28, pp. 229-245, 2003.

[23] M. Emami, J. Hansen, A. Kim, G. Papanicolaou, A. Paulraj, D. Cheung, and C. Prettie, "Predicted Time Reversal Performance in Wireless Communications Using Channel Measurements," *IEEE Communications Letters*, in press.

[24] M. Emami, M. Vu, J. Hansen, A. Paulraj, G. Papanicolaou, "Matched Filtering with Rate Back-off for Low Complexity Communications in Very Large Delay Spread Channels," in *Proc. Thirty-Eighth Asilomar Conference on Signals, Systems and Computers*, vol. 1, pp. 218-222, 2004.

[25] P. Kyritsi, C. Tsogka, G. Papanicolaou, "Frequency and antenna weighting schemes in time reversal communications," in preparation.

[26] L. Borcea, G. Papanicolaou, C. Tsogka, "Theory and applications of time reversal and interferometric imaging," *Inverse Problems*, vol. 19, pp. 5139-5164, 2003.


**Peter Blomgren** received his M.Sc. in Engineering Physics from the Royal Institute of Technology (Stockholm, Sweden) in 1994, and his Ph.D. in Mathematics in 1998 from the University of California Los Angeles. From 1998 through 2002 he was a research associate at Stanford University. He joined the faculty in the Department of Mathematics and Statistics at San Diego State University in the fall of 2002.

**Persefoni Kyritsi** received the B.S. degree in electrical engineering from the National Technical University of Athens, Athens, Greece, in 1996, the M.S. and the Ph.D. degrees in Electrical Engineering from Stanford University, Stanford, CA, in 1998 and 2002 respectively. She has spent time as an intern with Lucent Technologies Bell Labs, Deutsche Telekom, Intel and Nokia. From September 2003 until September 2005 she was visiting the Department of Mathematics at Stanford University. Since 2001, she has been with the Department Communication Technology in Ålborg University, Ålborg, Denmark, as an Assistant Professor.

**Arnold D. Kim** received his B.S. in Engineering Science and Applied Mathematics at Northwestern University, Evanston, IL in 1995. He received his M.S. and Ph.D. in Applied Mathematics at the University of Washington, Seattle, WA in 1997 and 2000, respectively. He was a postdoctoral fellow in the Department of Mathematics at Stanford University, Stanford, CA from 2000 to 2004. He joined the School of Natural Science at the University of California, Merced in the summer of 2004.

**George Papanicolaou** received his Ph.D. in Mathematics in 1969 from the Courant Institute of New York University. He joined the faculty of the Courant Institute where he was professor from 1976-1993. He has been professor of Mathematics at Stanford University since 1993.